Published in final edited form as:
J Org Chem. 2008 September 5; 73(17): 6480–6488. doi:10.1021/jo8008534.

Interaction Energies and Dynamics of Acid–Base Pairs Isolated in Cavitands

Byron W. Purse[†], **Sara M. Butterfield**[†], **Pablo Ballester**[‡], **Alexander Shivanyuk**[§], and **Julius Rebek Jr.**[*,†]

The Skaggs Institute for Chemical Biology and Department of Chemistry, The Scripps Research Institute, 10550 North Torrey Pines Road, La Jolla, California 92037, ICREA and Institute of Chemical Research of Catalonia (ICIQ), Avgda. Paisos Catalans s/n, 43007, Tarragona, Spain, Enamine Ltd., 23 A. Matrosova st., 01103 Kyiv, Ukraine, and National Taras Shevchenko University, 62 Volodymyrska st., Kyiv-33, 01033, Ukraine

Abstract

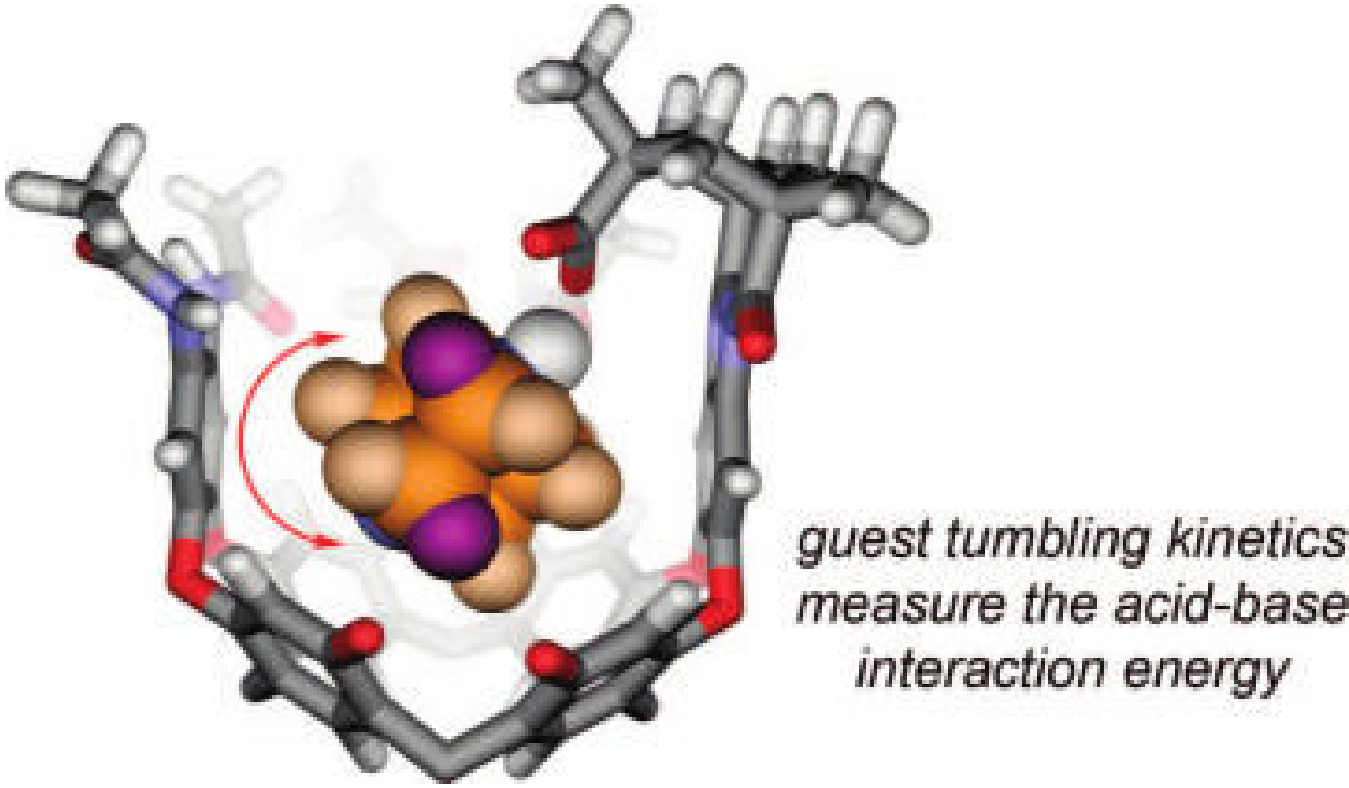

The use of capsules and cavitands in physical organic chemistry is briefly reviewed, and their application to the study of salt bridges is introduced. Carboxylate/ammonium ion pairs are generated within an environment that more or less surrounds the functional groups within a synthetic fixed

* To whom correspondence should be addressed. Tel: 858−784−2250. Fax: 858−784−2876 E-mail: jrebek@scripps.edu..
[†]The Scripps Research Institute.
[‡]ICREA and Institute of Chemical Research of Catalonia.
[§]Enamine Ltd. and National Taras Shevchenko University.

Supporting Information Available: General experimental, 2D ROESY spectrum showing exchange of DABCO in H**2a**, and a description of EXSY kinetic models. This material is available free of charge via the Internet at http://pubs.acs.org.

introverted solvent sphere. This is provided by cavitands that fold around amines and present them with a carboxylic acid function. Both organic and water-soluble versions were prepared, and their equilibrium affinities with quinuclidine bases were determined by NMR methods. The association constants range from approximately 10^3 M^{-1} in water to more than 10^5 M^{-1} in organic solvents. Studies of nitrogen inversion and tumbling of [2.2.2]-diazabicyclooctane within the introverted acids also illustrate the strength of the acid–base interactions. The barriers to in–out exchange of several amine guests were determined to be in the range from 15 to 24 kcal mol^{-1}. Some parallels with enzymes are drawn: the receptor folds around the guest species; presents them with inwardly directed functionality; and provides a generally hydrophobic environment and a periphery of secondary amide bonds.

Introduction

Molecular encapsulation offers a tool for probing functional group interactions in isolation. By temporarily confining a guest to a fixed space isolated from solution, a host molecule restricts the motions and conformations of its occupant and provides surroundings of ordered functionality. The host imposes an environment on the guest that is both physically and chemically distinct from the exterior solution. Many examples of encapsulation come from synthetic receptor design, and a growing literature describes the unique ability of hosts to control the properties of their guests.[1] Shifted equilibria of guest conformations[2] have been observed, and in some cases, guests have adopted previously unknown conformations, such as the coiled helical conformation of alkanes in shape-mismatched hosts.[3-5] New forms of isomerism[6] have arisen from the coencapsulation of multiple guests in the same host,[7] a consequence of the guests' positional arrangement or orientation or both.[8] Host molecules that more or less surround their guests can stabilize reactive species[9-12] by compartmentalization and geometric constraint,[13-19] but they can also increase the reactivity of guests[20-27] or change the rates[28,29] and selectivities of reactions that occur.[30-32]

Because the orientation, conformation, and motion of guests are subject to the constraints of the host, functional groups can be positioned in close proximity to the guest without the rapid exchange of partners that occurs in bulk solution. One approach involves the coencapsulation of multiple guests: hydrogen-bond-mediated functional group interactions have been studied in the context of enantioselection through coencapsulation.[33] The other approach, used in this work, is to affix the host molecule with inwardly directed functionality. Guest molecules are then selectively bound via complementary functional group recognition, and the interactions between functional groups of host and guest may be examined.

Here, we study the ability of host cavitands to isolate a carboxylic acid and an amine in a semirigid amphiphilic pocket of some 170 $Å^3$. Deep cavitands are open-ended vase-shaped hosts made up of an ordered arrangement of eight benzene groups and crowned with a hydrogen-bonded rim of up to eight secondary amides (Figure 1).[34-36] They are appropriately thought of as persistent solvent cages for which the entropic cost of organization has been paid during a covalent synthesis, and they reproduce some of the properties of the ordered hydrophobic interiors of proteins. Synthetic modifications of deep cavitands have placed functional groups on the upper rim; the ability of the resulting hosts to selectively bind guests and control their properties has been recently reviewed.[37] Of interest here are those cavitands, derived from Kemp's triacid, that direct a carboxylic acid rigidly toward the depths of their cavities.[38] Because of the architecture of these cavitands H**2**, any guest that is bound is forced to confront the carboxylic acid. The acid provides a complement to Lewis basic guests, but the structured environment surrounding the resulting acid–base pair has consequences in terms of energetics and dynamics. The cavitands H**2a** and H**2b** and their water-soluble counterpart H**2c** are examined as tools for studying acid–base interactions in isolation.

Results and Discussion

Cavitand Synthesis and Structure

The cavitands used in this study are synthetic extensions of the original "deep cavitands", which were prepared by multiple S_NAr reactions between a resorcin[4]arene and 1,2-difluoro-4,5-dinitrobenzene.[34] The best synthesis (in our hands) of hydrophobic introverted acid cavitands H**2a,b** was recently reported,[39] as has that for the water-soluble derivative H**2c**.[40] While the introverted acid cavitands synthesized and used in this study are racemic, it is possible to resolve the enantiomers by HPLC using a chiral column ((3*S*,4*R*) Pirkle 1J Regiscolumn, 4.6 × 250 mm, EtOH: CH_2Cl_2 (3:97), 1.0 mL/min). The water-soluble introverted acid host H**2c** was synthesized in a similar manner beginning from a Boc-protected amine-footed resorcin[4] arene.[40,41] Control acid H**3** was synthesized by the condensation of Kemp's triacid chloride anhydride with 1,2-dioctyloxy-4,5-diaminobenzene.[42]

The slow evaporation of a solution of H**2a** in chloroform resulted in the growth of crystals suitable for X-ray diffraction (Figure 2). In the crystalline state, the cavitand H**2a** adopts a distorted vase conformation. The resorcinarene framework adopts a nearly perfect crown conformation: the dihedral angles between the opposing resorcinol ring differ only by 5.3°. Three cavitand walls are nearly perpendicular to the main plane of the macrocycle (dihedral angles 89.9, 92.8, and 84.0°), whereas the fourth wall is tilted toward the cavity (the dihedral angle 72.4°). Four intramolecular hydrogen bonds are formed between the adjacent amide units; the other two involve the introverted carboxylic acid group. The C–O distances and the pattern of hydrogen bonds clearly indicate that the acid hydrogen atom is bound to oxygen O9. Neighboring molecules of H**2a** are associated through C=O–H–N hydrogen bonds (*d*(O13–N6) = 3.1 Å). In this way, 1D hydrogen-bonded molecular chains are formed in the crystal. While idealized model structures derived from molecular mechanics energy minimization (MM+ or AMBER) suggest an internal volume of 170 $Å^3$, the tilting of a wall of H**2a** reduces the cavity volume; this is an example of induced-fit binding.[43,44] The cavity volume in the X-ray structure, 145 $Å^3$, provides a snug fit for chloroform, with a packing coefficient of 0.51.[45,46] This value is close to the "ideal" of 0.55, typical for a wide array of hosts.[47] The distances between opposing walls are 5 and 6.5 Å, and the acid group is 5 Å from the bottom of the accessible cavity space. Such available space and host flexibility is suitable for the binding of one small molecule up to a maximum volume of around 120 $Å^3$. Chloroform bound inside H**2a** is oriented with its relatively polar C–H directed toward the aromatic ring of a cavitand wall. The CH–π interactions, as well as the stronger cation–π interactions, are major enthalpic contributors to the guest binding energy of cavitands of the types **1** and **2**,[48] and this is consistent with the orientation observed here. One chlorine atom is situated in the middle of the resorcinarene socket, forming close contacts with two resorcinol rings (3.4, 3.5 Å). Strong disorder of solvent molecules and high mosaicity of the crystal are responsible for high final *R* values.

The crystal structure reveals the strongly interactive nature of the carboxylic acid. Because chloroform offers a poor ability to make favorable intermolecular interactions with the acid, the cavitand's amide groups adapt to fill this role. The X-ray structure of C_4-symmetric deep cavitand **1b** shows the eight amide groups arranged in a ring of eight hydrogen bonds with a continuous clockwise or anticlockwise orientation.[36] In contrast, two of the corresponding interamide hydrogen bonds of H**2a** have been broken so that an NH is dedicated entirely to a hydrogen bond with the acid carbonyl. The acid OH participates in a hydrogen bond to an amide carbonyl on the wall opposite the NH donor; this carbonyl maintains a second hydrogen bond to another amide group of the upper rim. When a basic guest is present, the acid OH is otherwise occupied (vide infra), but it is worthwhile to mention that the donation of a hydrogen bond to the carboxylic acid is expected to increase the acidity.

While the X-ray structure described here is that of a cavitand with ethyl groups as “feet”, the results presented in this study as well as our experience with related cavitands clearly indicates that structural variation of these feet does not perturb the nature of the cavitand's binding pocket. Instead, the feet of the cavitand offer a site for modifications that can be used to control the solubility, attach fluorescent labels, or anchor the cavitand to a solid support.[41,49,50]

Amine Binding: Structure and Thermodynamics

Simple deep cavitands **1** bind small molecules of appropriate size and shape, including lactams and 1-substituted adamantanes, with binding energies that are typically on the order of $\Delta G° = 2-4$ kcal mol^{-1} in *p*-xylene-d_{10}.[34] Small amines such as triethylamine and quinuclidine are not particularly favored occupants of the cavity and are not bound appreciably in chloroform, which competes to occupy the inner space. When the cavitand is fitted with an introverted acid, as in H**2**, these amines are bound so tightly that the acid–base complex is stable to silica gel chromatography: the binding constants are $K_a > 10^5\ M^{-1}$. The structures of several complexes of H**2** and an amine guest have been studied previously using NMR.[38,42]

Numerous attempts to grow diffraction-quality crystals of complexes of H**2a** with DABCO and quinuclidine were unsuccessful. In order to reveal the geometrical features of inclusion complexes of these amines, model complexes with the more symmetrical octaamidocavitand **1a** were studied by single-crystal X-ray analysis.

Slow evaporation of a solution of **1a** and DABCO in mesitylene-d_{12} gave colorless crystals that were suitable for single-crystal X-ray analysis (Figure 3a), although they were unstable in the absence of the mother liquor. In the crystalline state, cavitand **1a** adopts a nearly ideal vase conformation: the dihedral angles between opposite pairs of resorcinol rings are 72.8 and 77.6°. The eight secondary amide groups form a cyclic array of hydrogen bonds, stabilizing this conformation. The clockwise or counterclockwise arrangement of amide groups makes the structure chiral. The unit cell contains both enantiomers, related by the center of symmetry (space group *P*1). The internal cavity of **1a** is occupied by one DABCO molecule, which takes a well-defined position. The dihedral angle between the planes of methylene groups adjacent to N11 and the rms plane of the four methine bridges of resorcinarene was found to be 33.7°. Of note is the absence of clear indications of strong, noncovalent interactions between host and guest. Only one short contact between a methylene carbon atom DABCO and a carbon atom of an aromatic cavitand wall (3.59 Å) indicates some weak noncovalent attraction. These observations are consistent with the observed weak binding of DABCO in solvents that compete to occupy the cavitand.

A similar slow evaporation of a solution of **1a** and quinuclidine in mesitylene-d_{12} also afforded diffraction-quality crystals. Single-crystal X-ray analysis revealed that the structure of cavitand molecule **1a** is nearly identical in both this complex and the complex of **1a** and DABCO (Figure 3b). Furthermore, the elemental cell parameters and crystal packing are nearly identical. The main differences between these structures lie in the orientation of guest molecules in the cavity of **1a**. One ordered quinuclidine molecule is situated in the cavity of **1a** with its methine C–H bond pointing toward the resorcinarene socket. The dihedral angle between the planes of the methylene groups adjacent to N9 and the plane of the four resorcinarene methine bridges (9.5°) is about three times smaller than the analogous value for DABCO. Quinuclidine is naturally less tilted in the cavitand's binding site. The subtle differences in size and electrostatic potential of the guests have a well-pronounced effect on their orientations when bound.

$^1H,^1H$ TOCSY NMR experiments on the complex of DABCO with H**2a** revealed $^3J_{H,H}$ coupling between quinuclidine methylenes and the proton shared by acid and base (Figures 4 and 5). This coupling indicates a bonding interaction between nitrogen and hydrogen, requiring a partial transfer of the proton to the base.[51,52] Carboxylic acids and amines hydrogen bond in

the gas phase, but the transfer of a proton is typical only in the liquid or solid states, in which the energy of solvation or the lattice energy stabilizes the charges.[53] The observation of $^3J_{H,H}$ coupling shows that the cavitand has some ability to stabilize an ion pair, which is consistent with the observed high affinity of deep cavitands for protonated tertiary amines and quaternary ammonium salts. This direct observation of a stabilized, hydrogen-bonded salt bridge in a cavitand interior is reminiscent of the stabilization of salt bridges in the hydrophobic interior of some proteins.

Competition experiments provide access to the interaction energy of the host acid and the guest amine, in a context suitable for the high association constants of amines and H**2a** in organic solvents (Figure 5). The unfunctionalized cavitand **1a** binds *N*-methylquinuclidinium tetrafluoroborate more strongly than it binds quinuclidine HCl (equilibrium A, $\Delta G°_A = -1.6 \pm 0.2$ kcal mol^{-1}). This observation is consistent with reported findings that cation–π interactions of quaternary ammoniums are typically stronger than those of the corresponding protonated amines.[54-56] In contrast, the introverted acid cavitand salt Na**2a** binds quinuclidine HCl more strongly than *N*-methylquinuclidinium tetrafluoroborate (equilibrium B, $\Delta G°_B = -3.1 \pm 0.1$ kcal mol^{-1}). Moreover, when unfunctionalized cavitand **1a** and introverted acid salt Na**2a** compete for quinuclidinium hydrochloride, Na**2a** binds it more tightly by $\Delta G°_D = -6.8 \pm 0.5$ kcal mol^{-1} (equilibrium D). The equilibrium lies too far to the side of quinuclidinium **2a** complex to measure directly by NMR and had to be calculated (Figure 6; eq 3). This value shows the increase in binding energy of quinuclidinium when a carboxylate is affixed to the host, and we interpret this energy as an approximate measure of the strength of the acid–base interaction.

A similar competitive binding experiment, offering both **1a** and Na**2a** to *N*-methylquinuclidinium tetrafluoroborate, revealed that host Na**2a** was preferred by $\Delta G°_C = -2.1 \pm 0.4$ kcal mol^{-1} (equilibrium C). The presence of the introverted acid functionality resulted in a significant increase in binding energy, but compared to the protonated quinuclidinium (equilibrium D), the difference was much smaller: $\Delta\Delta G° = 4.7 \pm 0.9$ kcal mol^{-1}. We cannot rule out that the larger size of the *N*-methyl guest causes repulsive interactions, but these cavitands have been shown to have a substantial ability to distend their walls and thereby accommodate larger occupants.[43] The other side of this flexibility is seen in the crystal structure of chloroform bound in H**2a** (Figure 1), where the walls of the host tilt inward in response to the relatively small size of the guest. It is more likely that the presence of the proton contributes to the binding energy through a hydrogen-bond-mediated salt bridge, a suggestion consistent with the observed $^3J_{H,H}$ ^{1}H NMR coupling.

It is of interest to compare the behavior of introverted acid H**2a** in organic solution with that of H**2c** in aqueous solution. The conformational behavior of H**2c** in D_2O is somewhat different from that of the organic-soluble versions. In the absence of an appropriate guest, Na**2c** adopts an open kite conformation with the aromatic walls of the host splayed outward.[57] Broadened, ill-defined proton resonances suggested any number of conformations, and even molecular aggregates in the free host that exchange at intermediate rates on the NMR time scale. Evidently, water is not a good enough guest, and the upper rim hydrogen bonds are not strong enough to hold the vase structure together in the competing aqueous solvent. The addition of a cationic guest, such as quinuclidinium hydrochloride, shifted the host equilibrium from the kite to the vase structure, through induced-fit recognition.[40] Similar guest-templated folding was observed previously for host **1c** in D_2O.[41]

Receptor Na**2c** bound quinuclidinium hydrochloride with an affinity of 1300 M^{-1} in buffered D_2O, an appropriate range to measure by NMR titration. In contrast, the nonfunctionalized receptor **1c** bound the same guest with a feeble association constant of 12 M^{-1}. A strongly favorable acid–base interaction exists in the complex formed with Na**2c**. By taking the

difference between the affinities of the introverted acid receptor Na**2c** and the octaamide receptor **1c**, an estimate of the buried salt bridge interaction is obtained: −2.7 ± 0.1 kcal mol^{-1} (cf. equilibrium D in Figure 6). While this method reasonably corrects for the interaction of the quinuclidinium cation with the host walls, as well as the desolvation of quinuclidinium, it does not account for the desolvation of the introverted carboxylic acid of the receptor, which occurs during the folding process. To address this problem, a "double mutant" cycle analysis[58-62] was performed (Figure 7). In complex A, the interaction between the introverted acid and the protonated amine guest is present. Complexes B and C represent the single mutants, whereby the interacting protonated amine has been methylated and the introverted acid has been removed, respectively. In order to prevent a possible charge–charge interaction in single mutant B, the measurement was carried out at pD 1.4 to protonate the carboxylic acid. Complex D represents the double mutant in which both interacting sites have been removed. The electrostatic interaction in the complex formed between $\mathbf{2c}^-$ and the quinuclidinium cation was accordingly determined to be −3.0 ± 0.4 kcal mol^{-1} using eq 4 (Figure 7).[58]

Amine Guest Exchange Kinetics and Host–Guest Complex Dynamics

In most examples, the nature of guest exchange of supramolecular complexes is determined predominately by the structural features of the host. Several mechanisms have been observed and are described in a recent review.[63] For deep cavitands of the types **1** and H**2**, the process of guest exchange is intrinsically tied to the processes of cavitand folding and unfolding. The "folded" cavitand is that which has its walls oriented as in the crystal structure (Figures 1 and 3). The unfolding process is an inversion of some of the nine-membered diether rings with concomitant breaking of interwall (i.e., interamide) hydrogen bonds; the result is a flattened conformation termed "kite".[57] While the two conformations, vase and kite, are well-known, recent studies by Diederich reveal that a hybrid structure is also possible.[64] In the early studies of deep cavitands **1** in organic solvents, it was found that the guest exchange energy, $\Delta G^{\ddagger}$ = 17 kcal mol^{-1}, had little dependence of the nature of the guest and was equal to the activation energy for cavitand unfolding.[34] In contrast, the rate of guest self-exchange in water-soluble cavitands does show a dependence on guest size.[4] The coupling of unfolding–folding to guest exchange is no surprise when one considers the alternative: a supramolecular S_N1 mechanism in which the guest is withdrawn through the cavitand's opening and a new guest (or a solvent molecule) enters by the reverse of this mechanism. Such a process necessarily entails desolvation of the entire inner surface of the cavitand and the creation of a transient vacuum of some 170 $Å^3$; this mechanism is expected only at high temperature and in systems that have no alternative.[65]

We performed EXSY NMR experiments on the diazabicyclo[2.2.2]octane (DABCO) complex of cavitand H**2a** and the *N*-ethyl-*N*-methyl-*N*-isopropylamine complex of H**2b**. In mesitylene-d_{12} solution, DABCO exchange in **1** operates by the unfolding–folding mechanism with nearly the usual activation energy, $\Delta G^{\ddagger}$ = 14.6 ± 0.4 kcal mol^{-1} at 300 K, as measured by EXSY NMR. This barrier is lower than the typical 17 kcal mol^{-1} because the high local concentration of the DABCO amine at the cavitand opening (or excess DABCO in solution) can facilitate the breaking of the interamide hydrogen bonds to "catalyze" unfolding. When bound by the introverted acid H**2**, exchange of DABCO could not be observed by EXSY NMR experiments because this process is too slow. An alternative method, in which we preformed a 1:1 complex of DABCO and H**2a** in mesitylene-d_{12} and then introduced 1 equiv of quinuclidine (which is a better guest), showed that the quinuclidine displaced the DABCO with $t_{1/2}$ = 27 min at 295 K, corresponding to $\Delta G^{\ddagger}$ = 22.0 ± 0.3 kcal mol^{-1}.[66] If the 5 K temperature difference is neglected, the presence of the introverted acid raised the barrier to exchange by 7.4 ± 0.5 kcal mol^{-1}, a value within experimental error of the 6.8 ± 0.5 kcal mol^{-1} change in thermodynamic binding energy described above (Figure 6, equilibrium D).

In the case of the *N*-ethyl-*N*-methyl-*N*-isopropylamine complex in $CDCl_3$, integration of the NOE cross-peaks provided the activation energy $\Delta G^{\ddagger} = 17 \pm 0.5$ kcal mol^{-1} for guest exchange, identical to that found for unfunctionalized cavitands **1**. This seemingly counterintuitive observation is explained if cavitand unfolding and the interruption (or exchange) of the acid–base interaction are not coupled in $CDCl_3$; that is, their energies are not additive. The cavitand unfolds like the unfunctionalized cavitand in a rate-limiting step, after which the acid is free to exchange partners rapidly.

During the exchange studies of DABCO, we noted the presence of NOE cross-peaks that correspond to chemical exchange between the DABCO methylene groups closer to the acid and those deeper in the cavity (Figure 8). This corresponds to "tumbling" of the guest. The EXSY measurements in either $CDCl_3$ or mesitylene-d_{12} showed that the barrier to tumbling was $\Delta G^{\ddagger} = 18 \pm 0.5$ kcal mol^{-1} at 300 K (see Figure S1 in the Supporting Information). The nature of the solvent did not appreciably influence this process; it appears to take place inside the cavitand. Typically, tumbling is much more facile in unfunctionalized cavitands, and the introverted acid functionality must control tumbling through its interaction with the guest. By cooling an NMR sample of DABCO bound to **1a**, a guest ^{1}H signal coalescence was observed at 230 K. Such coalescence is explained by either (1) slow racemization of the cavitand (the clockwise or counterclockwise arrangement of interamide H bonds; Figures 1 and 3) or (2) tumbling becomes slow on the NMR time scale. Option (1) is more likely because a similar coalescence is observed when quinuclidine is the guest and in this case tumbling does not occur. Therefore, the coalescence temperature for tumbling *is at most* 230 K, and the *maximum* barrier to tumbling is $\Delta G^{\ddagger} = 11.6 \pm 0.1$ kcal mol^{-1} in the unfunctionalized cavitand **1**. The difference between the DABCO tumbling process in **1** and H**2** is clearly attributable to the acid–base interaction. We propose that the difference in these barriers to tumbling, $\Delta\Delta G^{\ddagger} > 6.5 \pm 0.5$ kcal mol^{-1}, provides a minimum estimate for the interaction energy in the acid–base pair. This measurement is within experimental error of the $\Delta G° = 6.8 \pm 0.5$ kcal mol^{-1} measured in the thermodynamic cycle (Figure 6) and is consistent with the $\Delta\Delta G^{\ddagger} = 7.4 \pm 0.5$ kcal mol^{-1} value obtained from DABCO guest exchange observations.

The strength of this interaction energy profoundly affects the dynamics of the acid–base pair in H**2**. We reported the inversion dynamics of prochiral *N*-ethyl-*N*-methyl-*N*-isopropylamine bound by H**2b** and compared this process to that observed in the presence of simple carboxylic acids.[42] In CD_2Cl_2, control acid H**3** has the same influence as pivalic acid on *N*-ethyl-*N*-methyl-*N*-isopropylamine inversion. The barrier to inversion/rotation[67] of the amine is $\Delta G^{\ddagger} = 10.5 \pm 0.5$ kcal mol^{-1} in the presence of pivalic acid and $\Delta G^{\ddagger} = 10.3$ kcal mol^{-1} in the presence of H**3**. Introverted acid H**2**, on the other hand, formed complexes with *N*-ethyl-*N*-methyl-*N*-isopropylamine that had barriers to inversion/rotation that were too high to measure by EXSY NMR experiments, even at 323 K. Instead, the diastereomeric complexes interconvert by the lower barrier mechanism of guest exchange: the barrier to inversion/rotation inside the cavitand is greater than 24 kcal mol^{-1}! While a significant part of this raised barrier must come from the strength of the acid–base interaction, the cavitand provides a geometric barrier to the conformational changes intrinsic to this amine inversion. Together these properties are sufficient to suppress the inversion dynamics inside the cavitand.

Conclusions

The fusion of Kemp's triacid to deep cavitands results in host molecules with functionality trained on the guests inside. Convergent functions are not new in molecular recognition studies, and they can show high selectivities.[68,69] Even more effective would be assemblies such as capsules that completely surrounded the target and a functional molecule or two.[70,71] These introverted acids selectively bind amines of appropriate size and shape with binding constants on the order of $K_a = 10^3$ in water and $K_a > 10^5$ in organic solvents. While cation–π, CH–π, and

electrostatics contribute, a substantial component of binding energy comes from the acid–base interaction energy: −3 kcal mol^{-1} in water or −7 kcal mol^{-1} in organic solvents. The difference of 4 kcal mol^{-1} probably results from partial solvation of the acid–base interaction at the open top of the cavitand. Hydrogen bonding between acid and base stabilizes and influences the motions of the amine guest. For roughly spherical guests such as DABCO, the barrier to tumbling in the cavitand is raised by at least 6.5 kcal mol^{-1}. For the prochiral amine *N*-ethyl-*N*-methyl-*N*-isopropylamine, nitrogen inversion is not observed in the cavity. In some cases, the exchange of amine guests is slowed markedly by the acid: exchange of DABCO was slowed in mesitylene-d_{12}, and it was necessary to wash several times with 5 M HCl to completely extract quinuclidine from H**2a**. Together these results provide measurements of the interaction energy of acid–base pairs in isolation.

Experimental Section

X-ray Crystal Structure Determination

Crystallographic data were collected on a Siemens SMART[72] diffractometer equipped with a CCD area detector using graphite monochromatized Mo KR radiation [λ(Mo KR) = 0.71073 Å] radiation. Data in the frames corresponding to an arbitrary hemisphere of data were integrated using SAINT.[72] Data were corrected for Lorentz and polarization effects and were further analyzed using XPREP. An empirical absorption correction based on the measurement of redundant and equivalent reflections and an ellipsoidal model for the absorption surface was applied using SADABS. The structure solution and refinement were performed using SHELXTL[73] (refining on F^2).

Introverted acid H**2a** × 4.5 $CHCl_3$: measurements at 293 K, crystal size 0.4 × 0.3 × 0.3 mm, monoclonic, *P*2(1)/*c*, *a* = 12.507(3)Å, *b* = 31.341(8) Å, *c* = 26.083(6)Å, β = 94.522(5)°, *V* = 10192(4)$Å^3$, *Z* = 4, ρ_{calcd} = 1.346 g cm^{-3}, $2\Theta_{max}$ = 55.92°, μ = 0.431 mm^{-1}, *F*(000) = 4226, 364 parameters, *R*1 = 0.3179, *wR*2 = 0.6075 (for 7841 refl. $I > 2\sigma(I)$), *R*1 = 0.4608, *wR*2 = 0.6557 (for 22 154 unique reflections), *S* = 1.619, $\Delta\rho$ (min/max) = −0.721/0.933 e $Å^{-3}$.

1a · DABCO × $4C_9H_{12}$: measurements at 173 K crystal size 0.4 × 0.3 × 0.2 mm, triclinic, $P\bar{1}$, *a* = 15.413(1)Å, *b* = 18.268(1)Å, *c* = 22.201(2)Å, α = 91.5670(1)°, β = 107.567(1)°, γ = 114.4950(10)°, *V* = 5339.0(7) $Å^3$, *Z* = 2, ρ_{calcd} = 1.200 g cm^{-3}, $2\Theta_{max}$ = 56.04°, μ = 0.072 mm^{-1}, *F*(000) = 2046, 1383 parameters, *R*1 = 0.1123, *wR*2 = 0.2793 (for 17 655 refl. $I > 2\sigma(I)$), *R*1 = 0.1468, *wR*2 = 0.3040 (for 25 099 unique reflections), *S* = 1.105, $\Delta\rho$ (min/max) = −0.516/−1.049 e $Å^{-3}$.

1a · quinuclidine × $4C_9H_{12}$: measurements at 173 K, crystal size 0.3 × 0.2 × 0.2 mm, triclinic, $P\bar{1}$, *a* = 15.501(2)Å, *b* = 18.249(3) Å, *c* = 22.303(3) Å, α = 91.827(3)°, β = 107.458(3)°, γ = 114.319(3)°, *V* = 5396(1) $Å^3$, *Z* = 2, ρ_{calcd} = 1.187 g cm^{-3}, $2\Theta_{max}$ = 56.04°, μ = 0.079 mm^{-1}, *F*(000) = 2046, 1287 parameters, *R*1 = 0.1339, *wR*2 = 0.3283 (for 11 687 refl. $I > 2\sigma(I)$), *R*1 = 0.2204, *wR*2 = 0.3855 (for 22 927 unique reflections), *S* = 1.077, $\Delta\rho$ (min/max) = −0.81/1.06 e $Å^{-3}$.

Binding Constant Determination

Binding constants were determined by using an NMR titration that was optimized to show simultaneously resolved signals for cavitand, guest, and cavitand·guest complex. Solutions were prepared of the desired cavitand and guest at known concentrations in a deuterated NMR solvent. An initial spectrum of cavitand alone was recorded; the guest was then titrated, and new spectra were acquired until a point was reached where it was possible to accurately measure the integral area of peaks for the free cavitand, free guest, and the complex. The slow nature of guest exchange from these cavitands on the NMR time scale allows for these species to be

resolved in the spectrum. Spectra with good resolution of species were re-acquired using a 30 s pulse delay to improve the accuracy of integration of the signals for any species that might have a longer relaxation time, particularly the free guest. Binding constants were then calculated using eq 1.

$$K_a = \frac{[\text{cavitand} \bullet \text{guest}]}{[\text{cavitand}]\,[\text{guest}]} \quad (1)$$

Competitive binding experiments were performed by preparing, for example, a solution of host molecule with one guest present in a deuterated NMR solvent. A second, competing guest was then titrated in, and ^{1}H spectra were acquired until a significant portion of the first guest was displaced; this point is chosen somewhat arbitrarily but is placed in a range of good solubility and such that the relevant signals in the ^{1}H spectrum can be integrated accurately. The relative binding affinity K_{rel} is then calculated using eq 2.

$$K_{rel} = \frac{[\text{cavitand} \bullet \text{guest}\quad \text{B}]\,[\text{guest}\quad \text{A}]}{[\text{cavitand} \bullet \text{guest}\quad \text{A}]\,[\text{guest}\quad \text{B}]} \quad (2)$$

EXSY, TOCSY, and ROESY Measurements

^{1}H,^{1}H EXSY, ^{1}H,^{1}H TOCSY, ^{1}H,^{1}H NOESY, and ^{1}H,^{1}H ROESY experiments were performed at the temperatures and in the solvents indicated using standard pulse sequences. Exchange rates were measured with the 2D EXSY pulse sequence by integrating the relevant peaks of the 2D NOESY spectrum using XWINNMR followed by processing with D2DNMR software.[74]

Acknowledgment

We are grateful to the Skaggs Institute and the National Institutes of Health (GM 27932) for financial support. B.W.P. is a Skaggs Predoctoral Fellow, A.S. is a Skaggs Postdoctoral Fellow, and S.M.B. is a Ruth L. Kirschstein NRSA Fellow (F32 GM73437). We also thank Drs. Laura Pasternack and Dee-Hua Huang for assistance with NMR experiments.

References

1. Hof F, Craig SL, Nuckolls C, Rebek J Jr. Angew. Chem., Int. Ed 2002;41:1488–1508.
2. Iwasawa T, Mann E, Rebek J Jr. J. Am. Chem. Soc 2006;128:9308–9309. [PubMed: 16848447]
3. Schramm MP, Rebek J Jr. Chem.—Eur. J 2006;12:5924–5933.
4. Hooley RJ, van Anda HJ, Rebek J Jr. J. Am. Chem. Soc 2007;129:13464–13473. [PubMed: 17927175]
5. Hooley RJ, Rebek J Jr. Org. Lett 2007;9:1179–1182. [PubMed: 17323957]
6. Timmerman P, Verboom W, van Veggel FCJM, van Duynhoven JPM, Reinhoudt DN. Angew. Chem., Int. Ed. Engl 1994;33:2345–2348.
7. Heinz T, Rudkevich DM, Rebek J Jr. Angew. Chem., Int. Ed 1999;38:1136–1139.
8. Rebek J Jr. Angew. Chem., Int. Ed 2005;44:2068–2078.
9. Ziegler M, Brumaghim JL, Raymond KN. Angew. Chem., Int. Ed 2000;39:4119–4121.
10. Fiedler D, Leung DH, Bergman RG, Raymond KN. Acc. Chem. Res 2005;38:349–358. [PubMed: 15835881]
11. Kaanumalle LS, Gibb CLD, Gibb BC, Ramamurthy VJ. Am. Chem. Soc 2005;127:3674–3675.
12. Brody MS, Shalley CA, Rudkevich DM, Rebek J Jr. Angew. Chem., Int. Ed 1999;38:1640–1644.
13. Yoshizawa M, Kusukawa T, Fujita M, Yamaguchi KJ. Am. Chem. Soc 2000;112:6311–6312.
14. Kawano M, Kobayashi Y, Ozeki T, Fujita MJ. Am. Chem. Soc 2006;128:6558–6559.

15. Dong VM, Fiedler D, Carl B, Bergman RG, Raymond KN. J. Am. Chem. Soc 2006;128:14464–14465. [PubMed: 17090022]
16. Körner SK, Tucci FC, Rudkevich DM, Heinz T, Rebek J Jr. Chem.—Eur. J 2000;6:187–195.
17. Cram DJ, Tanner ME, Thomas R. Angew. Chem., Int. Ed. Engl 1991;30:1024–1027.
18. Iwasawa T, Hooley RJ, Rebek J Jr. Science 2007;317:493–496. [PubMed: 17656719]
19. Hooley RJ, Iwasawa T, Rebek J Jr. J. Am. Chem. Soc 2007;129:15330–15339. [PubMed: 18004856]
20. Purse BW, Ballester P, Rebek J Jr. J. Am. Chem. Soc 2003;125:14682–14683. [PubMed: 14640624]
21. Purse BW, Gissot A, Rebek J Jr. J. Am. Chem. Soc 2005;127:11222–11223. [PubMed: 16089433]
22. Richeter S, Rebek J Jr. J. Am. Chem. Soc 2004;126:16280–16281. [PubMed: 15600303]
23. McCurdy A, Jimenez L, Stauffer DA, Dougherty DA. J. Am. Chem. Soc 1992;114:10314–10321.
24. Stauffer DA, Barrans RE Jr. Dougherty DA. Angew. Chem., Int. Ed. Engl 1990;102:953–956.
25. Lee J-J, Stanger KJ, Noll BC, Gonzalez C, Marquez M, Smith BD. J. Am. Chem. Soc 2005;127:4184–4185. [PubMed: 15783196]
26. Heemstra JM, Moore JS. J. Am. Chem. Soc 2004;126:1648–1649. [PubMed: 14871092]
27. Hooley RJ, Rebek J Jr. J. Am. Chem. Soc 2005;127:11904–11905. [PubMed: 16117505]
28. Grotzfeld R, Branda N, Rebek J Jr. Science 1996;271:487–489. [PubMed: 8560261]
29. Hooley RJ, Biros SM, Rebek J Jr. Angew. Chem., Int. Ed 2006;45:3517–3519.
30. Yoshizawa M, Tamura M, Fujita M. Science 2006;312:251–254. [PubMed: 16614218]
31. Chen J, Rebek J Jr. Org. Lett 2002;4:327–329. [PubMed: 11820871]
32. Hooley RJ, Restorp P, Iwasawa T, Rebek J Jr. J. Am. Chem. Soc 2007;129:15639–15643. [PubMed: 18004852]
33. Scarso A, Shivanyuk A, Hayashida O, Rebek J Jr. J. Am. Chem. Soc 2003;125:6239–6243. [PubMed: 12785856]
34. Rudkevich DM, Hilmersson G, Rebek J Jr. J. Am. Chem. Soc 1998;120:12216–12225.
35. Rudkevich DM, Rebek J Jr. Eur. J. Org. Chem 1999:1991–2005.
36. Shivanyuk A, Rissanen K, Körner SK, Rudkevich DM, Rebek J Jr. HelV. Chem. Acta 2000;83:1778–1790.
37. Purse BW, Rebek J Jr. Proc. Natl. Acad. Sci. U.S.A 2005;102:10777–10782. [PubMed: 16043720]
38. Renslo AR, Rebek J Jr. Angew. Chem., Int. Ed 2000;39:3281–3283.
39. Iwasawa T, Wash P, Gibson C, Rebek J Jr. Tetrahedron 2007;63:6506–6511. [PubMed: 18612332]
40. Butterfield SM, Rebek J Jr. J. Am. Chem. Soc 2006;128:15366–15367. [PubMed: 17131990]
41. Haino T, Rudkevich DM, Shivanyuk A, Rissanen K, Rebek J Jr. Chem.—Eur. J 2000;6:3797–3805.
42. Wash PL, Renslo AR, Rebek J Jr. Angew. Chem., Int. Ed 2001;40:1221–1222.
43. Purse BW, Rebek J Jr. Proc. Natl. Acad. Sci. U.S.A 2006;103:2530–2534. [PubMed: 16477037]
44. Koshland DE Jr. Proc. Natl. Acad. Sci. U.S.A 1958;44:98–104. [PubMed: 16590179]
45. Guex N, Peitsch MC. Electrophoresis 1997;18:2714–2723. [PubMed: 9504803]
46. Nicholls A, Sharp KA, Honig B. Proteins 1991;11:281–296. [PubMed: 1758883]
47. Mecozzi S, Rebek J Jr. Chem.—Eur. J 1998;4:1016–1022.
48. Hof F, Trembleau L, Ullrich EC, Rebek J Jr. Angew. Chem., Int. Ed 2003;42:3150–3153.
49. Saito S, Rebek J Jr. Bioorg. Med. Chem. Lett 2001;11:1497–1499. [PubMed: 11412968]
50. Hauke F, Myles AJ, Rebek J Jr. Chem. Commun 2005:4164–4166.
51. Lyons BA, Montelione GT. J. Magn. Reson 1993;101:206–209.
52. Braunschweiler L, Ernst RR. J. Magn. Reson 1983;53:521–528.
53. Locke MJ, McIver RT Jr. J. Am. Chem. Soc 1983;105:4226–4232.
54. Ngola SM, Kearney PC, Mecozzi S, Russell K, Dougherty DA. J. Am. Chem. Soc 1999;121:1192–1201.
55. Rashkin MJ, Hughes RM, Calloway NT, Waters ML. J. Am. Chem. Soc 2004;126:13320–13325. [PubMed: 15479087]
56. Hughes RM, Waters ML. J. Am. Chem. Soc 2005;127:6518–6519. [PubMed: 15869257]

57. Moran J, Ericson J, Dalcanale E, Bryant J, Knobler C, Cram D. J. Am. Chem. Soc 1991;113:5707–5714.
58. Carter PJ, Winter G, Wilkinson AJ, Fersht AR. Cell 1984;38:835–840. [PubMed: 6488318]
59. Kato Y, Conn M, Rebek J Jr. J. Am. Chem. Soc 1994;116:3279–3284.
60. Park TK, Schröder J, Rebek J Jr. J. Am. Chem. Soc 1991;113:5125–5127.
61. Vaughan CK, Harryson P, Buckle AM, Fersht AR. Acta Crystallogr 2002;58:591–600.
62. Adams H, Carver FJ, Hunter CA, Morales JC, Seward EM. Angew. Chem., Int. Ed. Engl 1996;35:1542–1544.
63. Palmer LC, Rebek J Jr. Org. Biomol. Chem 2004;21:3051–3059. [PubMed: 15505705]
64. Gottschalk T, Juan B, Diederich F. Angew. Chem., Int. Ed 2007;46:260–264.
65. Tanner ME, Knobler CB, Cram DJ. J. Am. Chem. Soc 1990;112:1659–1660.
66. Calculated from the Eyring equation
67. The interconversion of the enantiomers of *N*-ethyl-*N*-methyl-*N*-isopropyl amine requires both the inversion of nitrogen and the rotation of a C-N bond. While the latter has a low activation energy in solution, this barrier may be raised considerably by geometric confines of the host
68. Galan A, de Mendoza J, Toiron C, Bruiox M, Deslongchamps G, Rebek J Jr. J. Am. Chem. Soc 1991;113:9424–9425.
69. Nowick JS, Ballester P, Ebmeyer F, Rebek J Jr. J. Am. Chem. Soc 1990;112:8902–8906.
70. Shivanyuk A, Rebek J Jr. Chem. Commun 2001:2424–2425.
71. Shivanyuk A, Rebek J Jr. Chem. Commun 2001:2374–2375.
72. Siemens Industrial Automation, I. SMART, Area Detector Software Package. Siemens; Madison, WI: 1995.
73. Sheldrick, G. Siemens Industrial Automation, I. Siemens; Madison, WI: 1993.
74. Abel EW, Coston TPJ, Orrell KG, Sik V, Stephenson D. J. Magn. Reson 1986;70:34–53.

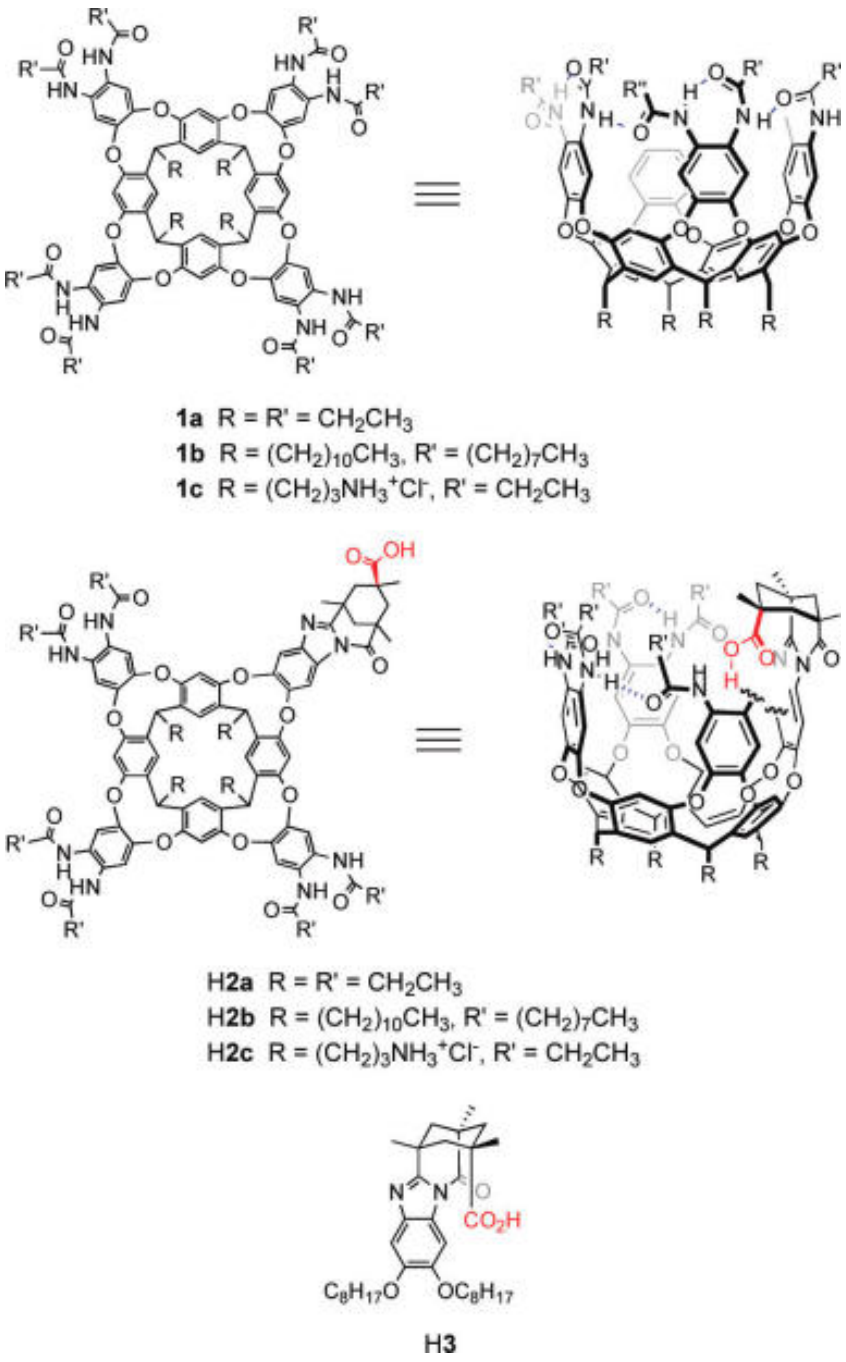

FIGURE 1.
Deep cavitands **1**, introverted acid cavitands H**2**, and control molecule H**3**.

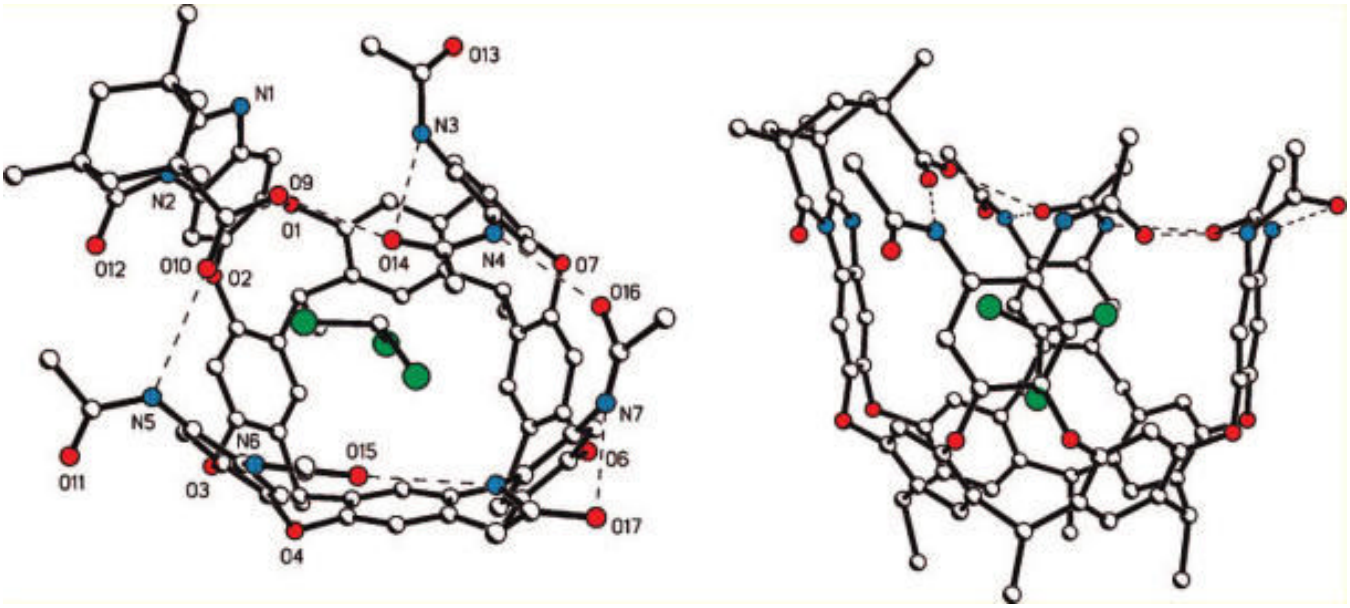

FIGURE 2.

Side and top views of the X-ray crystal structure of introverted acid H**2a** with bound chloroform. Ethyl groups have been shown as methyl groups for clarity. Hydrogen bonds are shown as dashed lines.

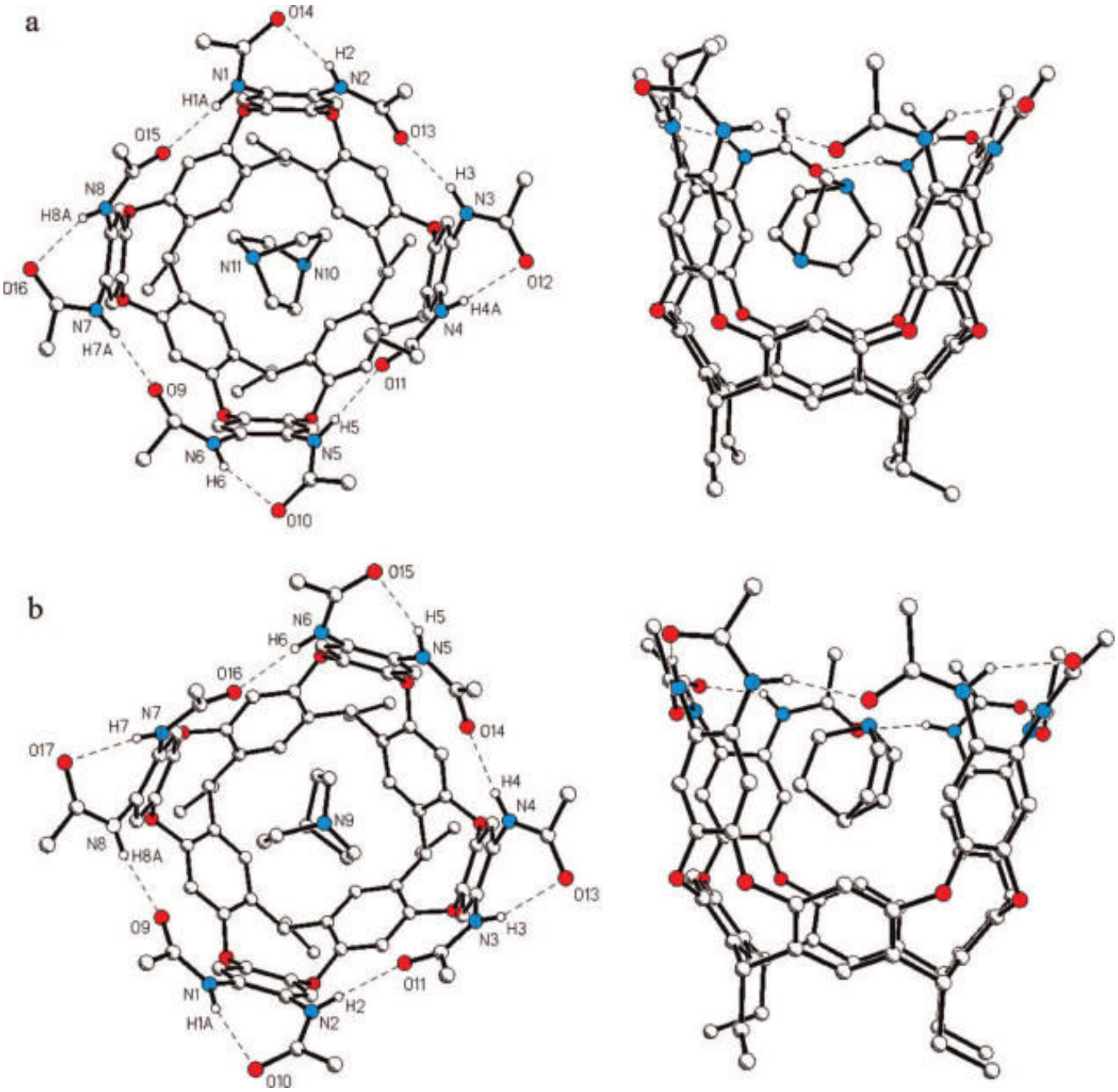

FIGURE 3.

Top and side views of the X-ray crystal structures of octaamide cavitand **1a** with bound DABCO (a) and with bound quinuclidine (b). Hydrogen bonds are shown as dashed lines, and methyl groups have been truncated from propionamides.

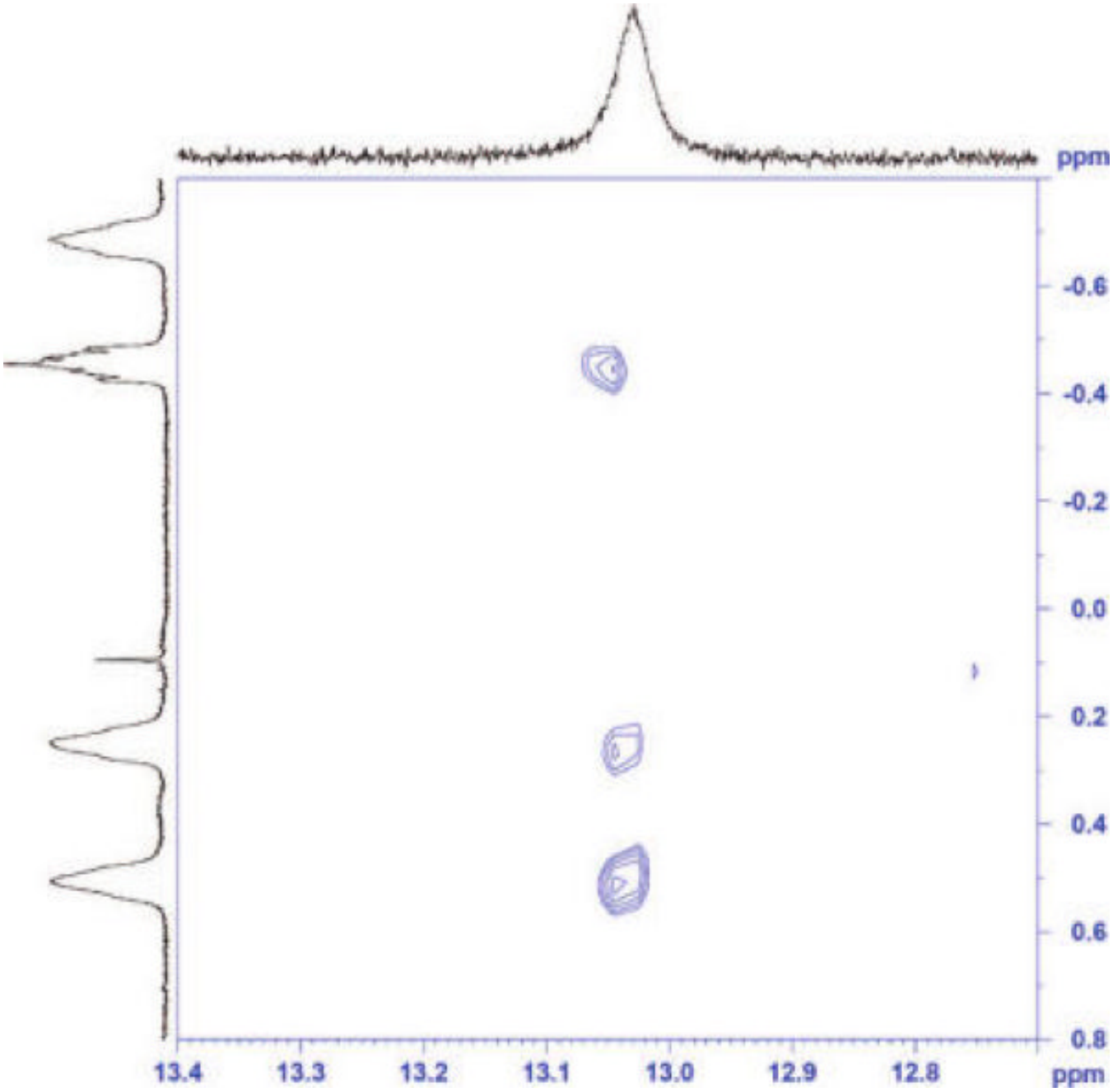

FIGURE 4.

$^{1}H,^{1}H$ TOCSY spectrum ($CDCl_3$, 298 K) showing $^{3}J_{H,H}$ coupling between the DABCO methylene protons and the proton shared by the base and the acid of host H**2a**. This coupling reveals that the acid proton has been at least partially transferred to a nitrogen of DABCO.

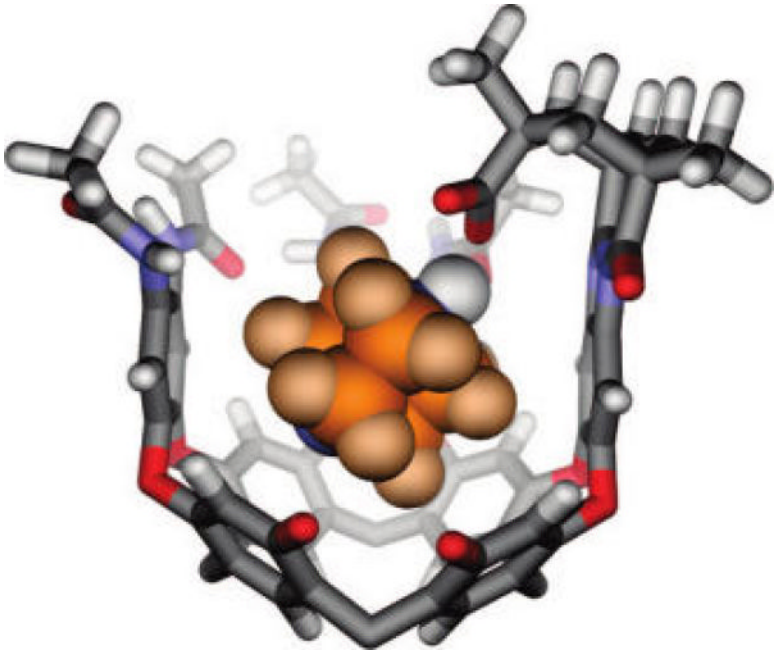

FIGURE 5.

Modeled structure (HyperChem; MM+ force field) of DABCO bound by H**2a**. Ethyl groups have been truncated or shown as methyl groups, and one cavitand wall has been removed for clarity. The acid proton (shown in white, CPK style) has been transferred to DABCO, consistent with TOCSY measurements.

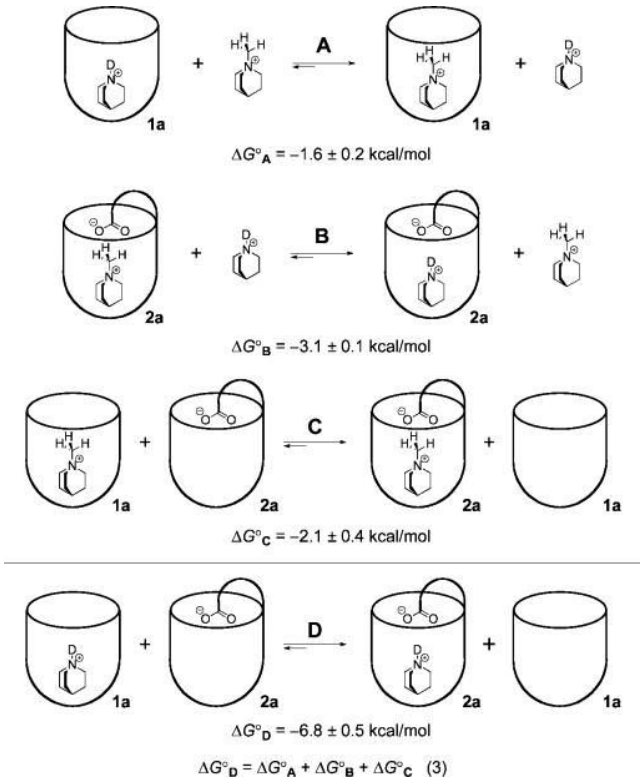

FIGURE 6.

Competitive binding experiments elucidate the guest binding preference of each host (A and B) and the preferred host selection of each guest (C and D). Equilibrium D provides an estimate of the interaction energy of the quinuclidinium–carboxylate pair, $\Delta G°_D = 6.8 \pm 0.5$ kcal mol^{-1}. $\Delta G°$ values for A, B, and C were determined by ^1H NMR titration in 5% CD_3OD in $CDCl_3$, and $\Delta G°_D$ was calculated according to the eq 3. Free sodium cations, tetrafluoroborate anions, and chloride anions are not shown.

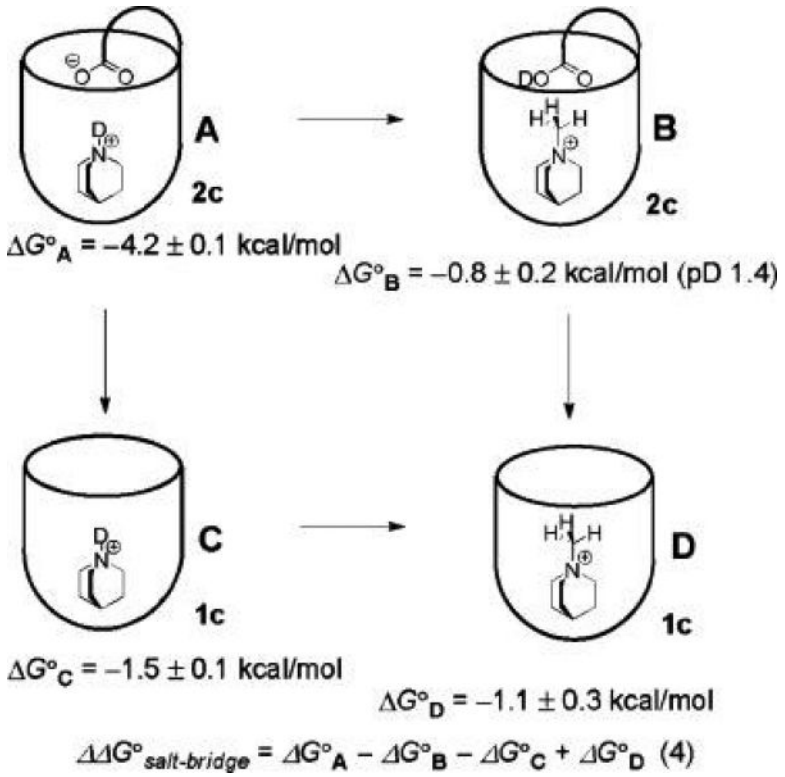

FIGURE 7.

Free energy cycle in deuterated water. Δ*G*° values refer to the binding energy of each host–guest complex as shown schematically. Measurements were performed at 300 K in 10 mM sodium phosphate buffer, pD 5.25, except where indicated.

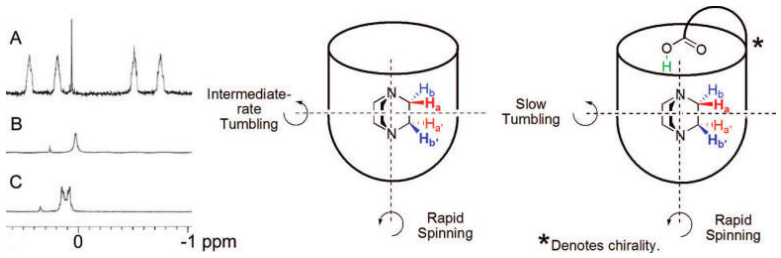

FIGURE 8.

In the unfunctionalized cavitand (center), DABCO spins rapidly about the vertical axis and tumbles at a slower rate about a horizontal axis. The introverted acid cavitand H**2** has no appreciable effect on spinning, but tumbling is dramatically slowed. The ^{1}H NMR spectrum of DABCO bound by **2** (A) shows four distinct signals for the guest, the further upfield signals $H_{a'}$ and $H_{b'}$ corresponding to the methylenes deeper in the cavitand. DABCO bound by **1** shows only a single guest peak at 300 K (B), but separate signals are seen at 220 K (B); the coalescence temperature was 230 K.